FINAL TECHNICAL REPORT

DEFORMATION AND EARTHQUAKE POTENTIAL OF THE EASTERN COAST RANGES FROM PS-INSAR MEASUREMENTS

Principal investigator:

Roland Bürgmann

University of California, Berkeley
Department of Earth and Planetary Science
307 McCone Hall
Berkeley, CA 94720-4767
Telephone: (510) 643-9545;
Fax:(510) 643-9980;
e-mail: burgmann@seismo.berkeley.edu

Deformation and Earthquake Potential of the Eastern Coast Ranges from PS-InSAR Measurements

Award Number: **08-HQGR-0095**

Roland Bürgmann
University of California, Berkeley
Department of Earth and Planetary Science
307 McCone Hall
Berkeley, CA 94720-4767
Telephone: (510) 643-9545;
Fax:(510) 643-9980;
E-mail: burgmann@seismo.berkeley.edu

Technical Abstract:

This investigation aims to constrain rates of vertical motion and interseismic strain accumulation in the Eastern Bay Area using Permanent Scatterers in InSAR (PS-InSAR). Range change rates determined with InSAR allow us to resolve tectonic surface motions at specific locations at great precision. The PS-InSAR dataset reveals variations in creep along the Concord fault. Creep rates decrease from south to north along the fault, with a maximum of 4.8 ± 0.7 mm/yr near the locations of two alinement arrays. The geodetic measurements also put constraints on the amount and patterns of uplift, which provide information on their origin (groundwater, tectonic or otherwise). In the Vacaville and Mount Diablo regions, vertical motions related to changes in groundwater level tend to be of greater magnitude than tectonic motions and can have both seasonal and longer-term components. This can have the effect of obscuring the tectonic signal, though in Mount Diablo we can constrain the tectonic uplift rate to be no more than 0.6 ± 1.0 mm/yr. In the San Joaquin/Sacramento Delta region, non-tectonic subsidence is pervasive, with rates of up to 10 mm/yr. PS points locate both along the levee walls and within the islands and all show steady subsidence.

Non-technical Abstract:

The Permanent Scatterer technique for using satellite radar interferometry (PS-InSAR) allows us to resolve surface motions in the Eastern San Francisco Bay Area and San Joaquin/Sacramento Delta region at great precision. The space geodetic measurements provide information about the rate at which faults slip and about the magnitudes of subsidence and uplift. In the Eastern Bay Area, tectonic rates of uplift are slow, not more than 0.6 ± 1.0 mm/yr. Non-tectonic vertical motions are larger, but show strong seasonal variation and are a mix of uplift and subsidence. In the San Joaquin/Sacramento Delta region, longer-term subsidence is pervasive on both the levees and islands.

DEFORMATION AND EARTHQUAKE POTENTIAL OF THE EASTERN COAST RANGES FROM PS-InSAR MEASUREMENTS

1. INTRODUCTION

Transform motion along the San Andreas plate boundary zone in California is partitioned between major right-lateral strike-slip faults that accommodate most of the total plate motion, including structures along the eastern edge of the California Coast Ranges around the rapidly developing San Joaquin-Sacramento Delta region (Figure 1). Of the approximately 49 mm/yr of relative plate motion, about 40 mm/yr are distributed across the San Andreas fault (SAF) system, with the remainder occurring east of the Great Valley-Sierra Nevada region [e.g. *Argus and Gordon*, 2001; *d'Alessio, et al.*, 2005; *Murray and Segall*, 2002]. Contraction across the SAF system is evident in the Neogene development of uplifted, folded, and thrusted terrain of the California Coast Ranges and in the occurrence of earthquakes with thrust components (e.g., the M > 6 Vacaville - Winters 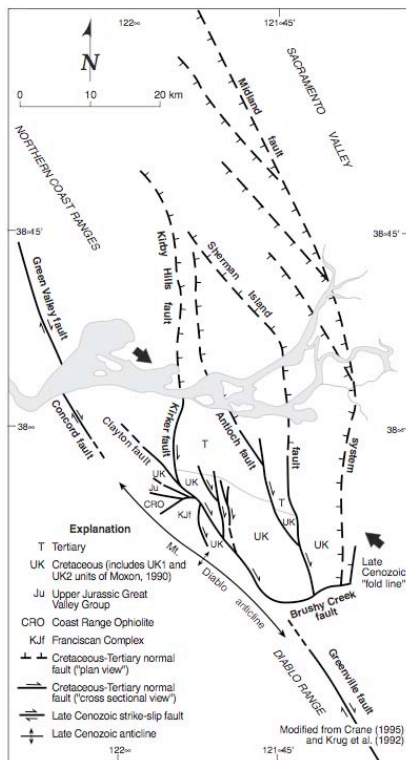earthquakes in 1892, and Coalinga, Kettleman Hills, Whittier Narrows, Loma Prieta, Northridge, and San Simeon events). The M ~6.5 April 19, 1892 Vacaville – Winters earthquake (Figure 2) resulted in intensity VII or greater damage throughout most of Yolo and Solano counties and may have ruptured the buried Gordon Valley, Midland or some other unidentified blind thrust fault along the Coast Range front [*Bennett*, 1987; *O'Connell, et al.*, 2001]. None of California's historic thrust earthquakes produced clear surface scarps that would be accessible to paleoseismic investigations, and the hazard characterization of such buried seismic sources based on traditional geologic and geophysical investigations is difficult. The two main causes for contractional tectonics along the transform plate boundary are a component of convergence across the Pacific-North American plate margin since ~3.5 Ma [e.g. *Page, et al.*, 1984], and "restraining" discontinuities along the strike-slip fault system such as steps and bends [e.g. *Aydin and Page*, 1984]. Regional plate-normal convergence across the Bay Area is estimated at 2-4 mm/yr [e.g., *Argus and Gordon*, 2001]. Examples of localized contraction include a 10° bend of the SAF through the Santa Cruz Mountains, the step-over region between the Calaveras and Hayward faults, and a left step-over between the Greenville and Concord faults (creating Mt.

Figure 1. Regional fault map of Sacramento-San Joaquin Delta region showing the Green Valley, Concord and Greenville faults and extent of buried range front thrust faults (Unruh and Dumitru, [2007]).

Diablo). Convergence across thrust faults in these areas may reach 5 mm/yr [*d'Alessio, et al.*, 2005].

Prescott et al. [2001] and *Murray and Segall* [2002] infer that much of the regional convergence may be accommodated by active contractional structures along the eastern margin of the Coast Ranges, as evidenced by a zone of localized convergence in GPS velocities. However, recent analyses by *Savage et al.* [2004] and *d'Alessio et al.* [2005] suggest that estimates of regional convergence accommodated by these structures are highly sensitive to assumptions of the geometry of the major fault zones. Some or all of the plate-boundary-normal strain in the Bay Area may be accommodated by more northerly striking strike-slip faults, such as the Calaveras and Mt. Lewis fault zones.
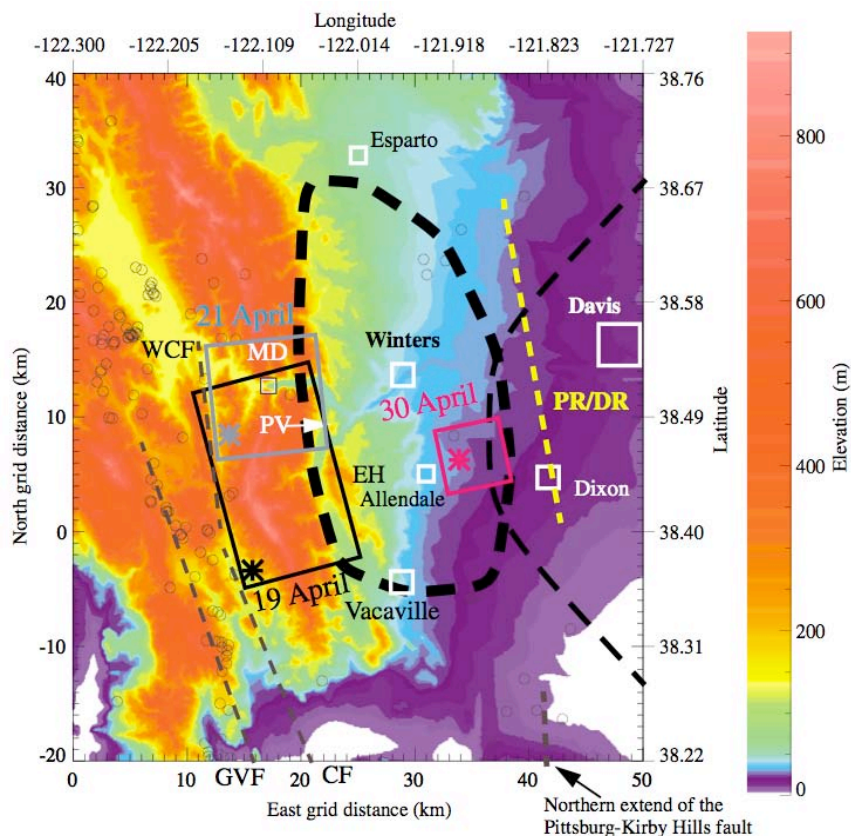

Figure 2. Color-shaded topography of northern Delta region. Black and blue lines show surface projection of the two segments of the Gordon Valley thrust fault postulated to have ruptured on 19 April 1892 (M 6.5) and 21 April 1892 (M 6.2). The location of a 30 April M 5.5 aftershock is shown in magenta and 1982-1998 microearthquakes are grey circles. Dashed grey lines show other faults, including the northern terminus of the Pittsburg-Kirby Hills fault (based on seismicity), and the Green Valley (GVF), Cordelia (CF), and Wragg Canyon (WCF) strike-slip faults. From *O'Connell et al.*, [2001].

In the past, geodetic data have been successfully used to infer fault slip rates, locking depths and distribution of aseismic slip on the major strike-slip faults in the San Francisco Bay Area. However, this approach has generally been unsuccessful in constraining the geometry and rates of contractional structures in the region. This is predominantly due to the low deformation rates typically associated with these structures, the superposition with the regional strike-slip deformation field, incomplete knowledge of the deep geometry of these faults, and the apparent effect of non-tectonic processes (e.g., land subsidence and rebound, sediment settling, and landslides).

1.1 Deformation Along the Eastern Coast Ranges and the San Joaquin-Sacramento Delta

Measurements of interseismic deformation provide valuable information about the rate of elastic strain accumulation and allow us to estimate slip rates of major faults in a tectonically active region. Much work has focused on and illuminated deformation rates across the major strike-slip faults, with a recent analysis funded by the NEHRP program summarizing progress in this effort [*d'Alessio, et al.*, 2005]. Continued improvements in the extent and precision of horizontal deformation measurements using GPS, such as made possible by the ongoing addition of PBO CGPS stations, will further improve our ability to model strike-slip rates on major faults throughout central California.
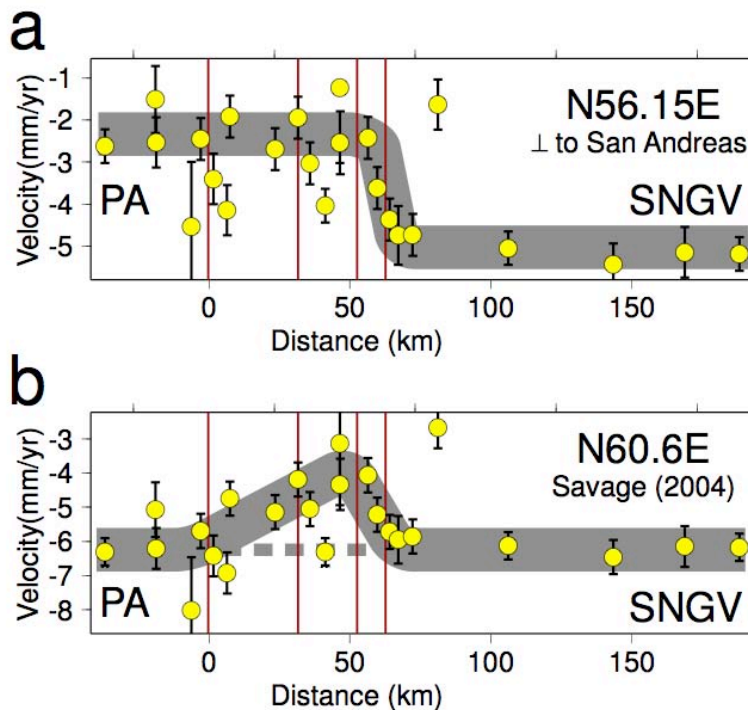

Figure 3. Effect of profile orientation on convergence estimates. Top panel shows the profile-perpendicular component of velocities from the northern Bay Area oriented N56.15°E, perpendicular to the strike of the San Andreas fault. Bottom panel shows profile-perpendicular velocities projected onto a slightly different orientation, N60.6°E (the orientation of maximum extension from *Savage et al.* [2004]). The orientation perpendicular to PA-SNGV motion at this latitude from the preferred model of d'Alessio et al. [2005] is N59.6°E. Thick grey bands show possible interpretations of the data [see *d'Alessio, et al.*, 2005].

Abundant folds and thrust faults roughly parallel to the San Andreas system suggest that pure strike-slip motion on the major Bay Area faults does not accommodate all of the plate boundary motion. *Savage et al.* [1998] used EDM trilateration measurements collected over nearly 20 years to determine the regional strain field in the Bay Area. They find that the Bay Area as a whole undergoes an insignificant amount of areal dilatation, but identify localized zones where contraction would give rise to thrust faulting, such as the region around the 1989 Loma Prieta rupture. In contrast to the trilateration work, some studies suggest that Bay Area GPS data require a component of fault-normal contraction between the SNGV block and the Bay Area. *Prescott et al.* [2001] analyze a profile between Point Reyes and Davis and find 3.8 ± 1.5 mm/yr of shortening over a 25-km-wide zone localized at the margin of the Great Valley. For a similar time span and data covering a larger range of latitudes in the Bay Area, *Murray and Segall* [2001] find 2.4 ± 0.4 mm/yr of contraction accommodated over a similarly narrow (<15 km) zone. *Freymueller* et al. [1999] present data from further north and conclude that shortening

must be less than 1-3 mm/yr. *Pollitz and Nyst* [2005] fit regional GPS data with a viscoelastic model and find 3 mm/yr of shortening perpendicular to the PA-SNGV relative plate velocity. *Savage et al.* [2004] prefer an interpretation where there is uniform contraction across the entire Coast Range.
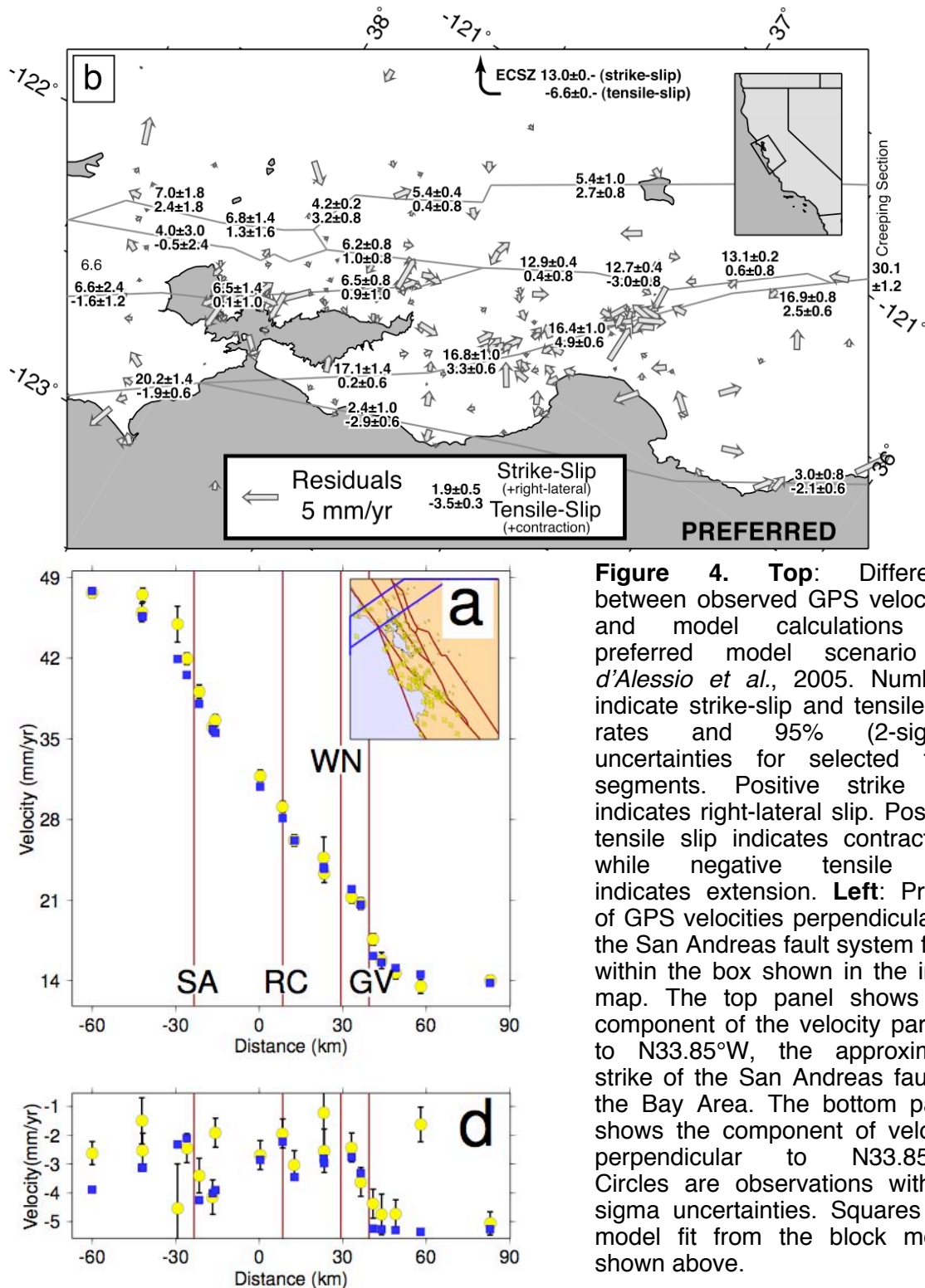

Figure 4. Top: Difference between observed GPS velocities and model calculations for preferred model scenario of *d'Alessio et al., 2005*. Numbers indicate strike-slip and tensile-slip rates and 95% (2-sigma) uncertainties for selected fault segments. Positive strike slip indicates right-lateral slip. Positive tensile slip indicates contraction, while negative tensile slip indicates extension. **Left**: Profile of GPS velocities perpendicular to the San Andreas fault system from within the box shown in the inset map. The top panel shows the component of the velocity parallel to N33.85°W, the approximate strike of the San Andreas fault in the Bay Area. The bottom panel shows the component of velocity perpendicular to N33.85°W. Circles are observations with 1-sigma uncertainties. Squares are model fit from the block model shown above.

Investigations of convergence in the Coast Range are commonly based on the presentation and interpretation of profiles across the plate boundary, such as we show for BAVU in Figures 3 and 4b (e.g., Fig. 2 of Murray and Segall [2001]; Fig. 5 of Prescott et al. [2001]; Fig. 4 of Savage et al. [2004]). These plots show the two horizontal components of GPS velocity projected onto a coordinate system with axes parallel and perpendicular to an "average" plate boundary orientation (usually parallel to the PA-NA relative motion and not PA-SNGV). The shape of the profile is highly dependent on the choice of the orientation used to define this average. Because the deformation field is projected onto a single orientation, pure strike-slip motion on faults with a range of orientations can yield an apparent "fault-normal contraction" signal. Figure 3 shows GPS data from the North Bay profile perpendicular to the San Andreas fault (N33.85W, Fig. 3a) and the azimuth of maximum shear strain from *Savage et al.* [2004] (N29.4W, Fig. 3b). When accounting for the formal uncertainties, both profiles are statistically permissive of a scenario with no net convergence. The systematic pattern in both plots, however, implies that the variations are not random scatter. In the first profile, there is an abrupt step in the data at the Green Valley fault, suggesting ~2 mm/yr of contraction between the Pacific and SNGV plates accommodated near that structure, just to the west of the proposed source rupture of the 1892 earthquake (Figure 2, *O'Connell et al.*, [2001]).

We use a block model [*d'Alessio, et al.*, 2005] to more rigorously constrain the magnitude and location of fault-perpendicular convergence and calculate the relative motion vector for individual blocks within the Bay Area directly. The grey vectors in Figure 4a show the orientation and magnitude of relative motion that is accommodated by faults in our preferred model. In the figure, we hold the eastern side of each fault fixed. The vectors show that relative motion is, in general, nearly parallel to local fault strike. Resolving these vectors onto the local fault orientation indicates how much convergence must be accommodated. For example, the bend in the San Andreas fault at the Santa Cruz Mountains shows as much as 4.9 ± 0.6 mm/yr of contraction perpendicular to the segment (likely accommodated by a number of thrust faults alongside the San Andreas fault). Our preliminary analysis shows that along the eastern margin of the Diablo Range, the Valley Margin deformation zone converges by 2.7 ± 0.8 mm/yr. The block modeling requires a similar magnitude of convergence across the Concord/Green Valley fault system in addition to the modeled ~7 mm/yr strike-slip rate on those faults. If we treat the Concord/Green Valley and West Napa fault systems together we find 1.9 ± 3.0 mm/yr of convergence (Figure 4). In general, motions east of the Bay are slightly clockwise of the faults, indicating convergence. This is balanced by a slight extensional component west of the Bay. We therefore agree with the assertion by *Savage et al.* [2004] that there is minimal net convergence across the Bay Area. PS-InSAR analysis allow us to further refine our knowledge of the deformation field and explore details of the vertical motions at a precision not accessible to GPS analysis.

2. PS-InSAR DATA

Standard InSAR measurements that rely on one or a stack of several interferograms are often hampered by significant noise introduced by atmospheric delays (often equivalent to several cm of surface motion) and by loss of coherence in vegetated or high-relief terrain. A new InSAR processing technique, the Permanent Scatterer method [PS-InSAR, *Colesanti, et al.*, 2003; *Ferretti, et al.*, 2004; *Ferretti, et al.*, 2000, 2001] allows for the identification and integration of individual phase-stable points (outcrops, buildings, utility poles, etc.) in all SAR images of an area of interest. Instead of using spatial averaging, filtering, or stacking of interferograms, the PS-InSAR method identifies individual radar-bright and radar-phase-stable pixels (i.e., permanent scatterers of incident radar) that exist within a radar scene and uses these reliable targets to separate surface motions from atmospheric and elevation error components of the range-change measurement.

The permanent scatterer approach works particularly well over urban areas, where an abundance of man-made structures results in large numbers of suitable radar-bright and phase-stable reflectors, but also usually identifies points in more remote areas that are considered unsuitable for standard InSAR, such as in the vegetated and uplifted regions we will focus on. The PS-InSAR method can measure surface motions at a level of < 1 mm/yr and can resolve
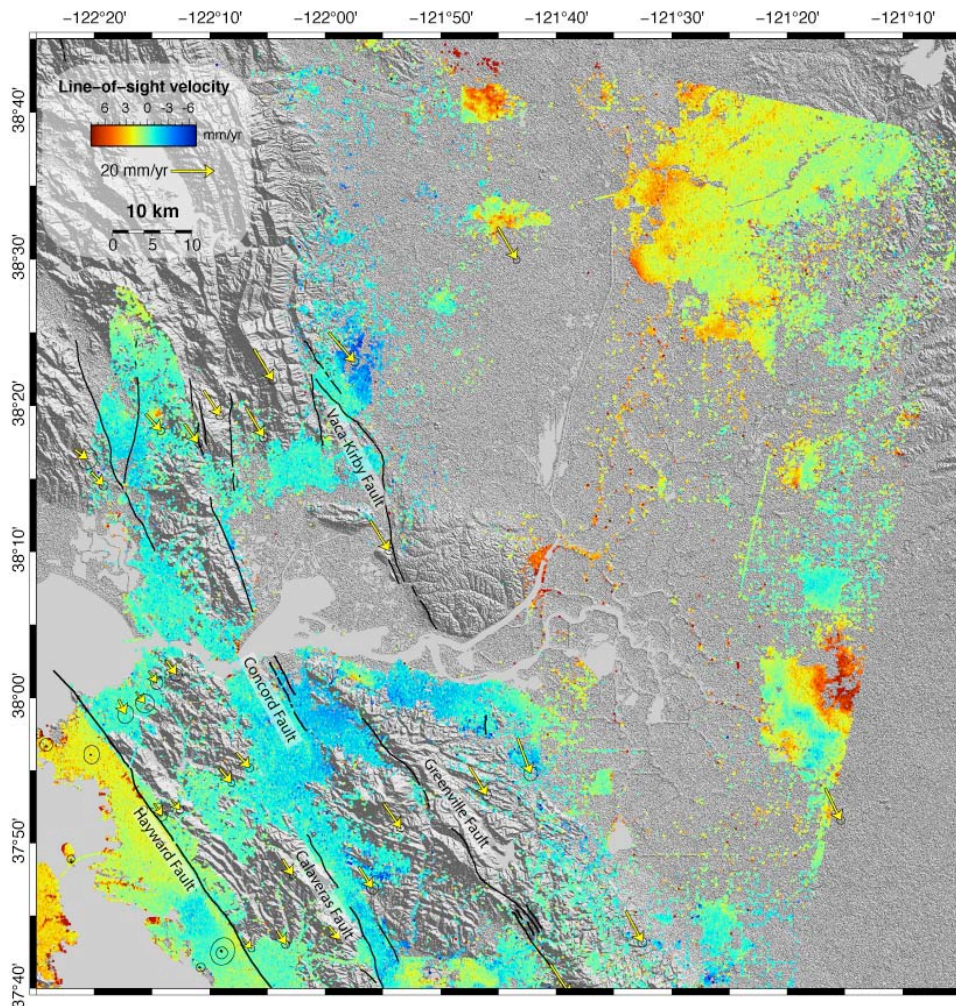
Figure 5: PS-InSAR data spanning eastern Coast Ranges and Great Valley. Note uplift feature (negative LOS velocity) near Vacaville and rapidly subsiding areas in Valley. Sharp offsets across Hayward, Concord, and Green Valley faults (black lines) are due to fault creep. Yellow arrows show horizontal GPS velocities from BAVU compilation.

very small-scale features, including motions of individual scatterer targets [e.g. *Colesanti, et al.*, 2003] not previously identified by conventional SAR interferometry over the San Francisco Bay Area. To date, we find that only permanent scatterer methods allow for measurements spanning the whole region we focus on [*Bürgmann, et al.*, 2006], provide sufficient spatial resolution to recognize and account for spatially complex non-tectonic motions [*Ferretti, et al.*, 2004; *Hilley, et al.*, 2004], and achieve a precision of the obtained range-change time series and rates that allows us to resolve sub-mm/yr displacement rates and detect mm-level deformation events [*Colesanti, et al.*, 2003].

InSAR provides a one-dimensional measurement of change in distance along the look direction of the radar spacecraft. Given the orientation of the track direction of polar, sun-synchronous satellites, this measurement is affected by deformation in both horizontal components and, particularly, in the vertical. We used 46 acquisitions of a descending orbit scene covering 1992 to 2000, collected by the ESA spacecraft ERS 1 and 2 flying north to south on track 70, frame 2853 (Figure 5).

3. RESULTS

3.1 Uplift near the Vaca-Kirby fault

A notable region of uplift is evident in the PS-InSAR dataset near the Vaca-Kirby fault in the North Bay Area. The feature is particularly notable because it has a linear boundary close to the Vaca-Kirby fault. To investigate whether this feature has a tectonic origin, we look at both the time dependence of ground movement and the pattern of deformation along a profile trending perpendicular the Vaca-Kirby fault. We use swath averaging to decimate the data within the dashed box of Figure 6 and construct profiles of ground motion for each acquisition date in the PS-InSAR dataset. The swath area is divided into 0.25 km wide bins, spanning the width of the area and arranged perpendicular to the profile. PS points within each bin are averaged together and projected onto the profile's centerline.
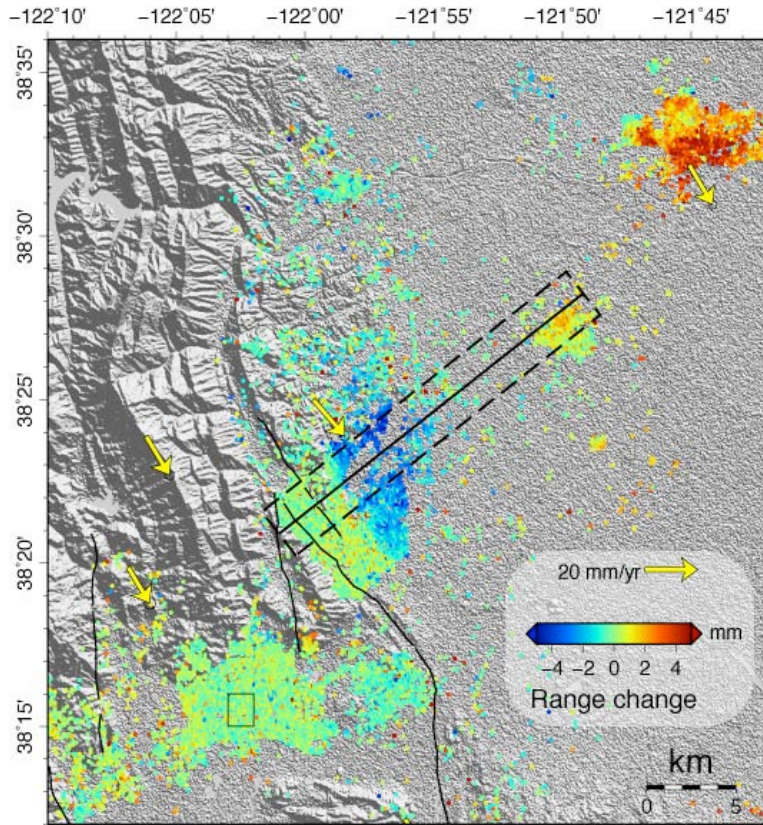

Figure 6: Map view with shaded topography of Vacaville area, showing velocity of PS-InSAR points as colored circles. Yellow arrows are BAVU GPS velocities. Dashed box shows area used for swath averaging.

The Vacaville profile contains two distinct regions with time-dependences of motion (Figure 7). From 4 – 12 km, the profile shows steady uplift with little seasonal variability, while from 18 – 22 km seasonal variability dominates. This can be seen in the time series for two points in the Vacaville profile (Figure 8). Point 23 shows monotonic uplift at a rate of ~4 mm/yr until 1997, after which the uplift rate decreases and seasonal cycles become somewhat more pronounced. This is a much larger uplift rate than would be expected given a convergence rate of 2.4 ± 1.8 mm/yr determined by *d'Alessio et* al. [2005] in this area. Sample 75 shows much more pronounced seasonal cycles than sample 23 throughout the dataset's time span and it motion seems to be more clearly influenced by fluctuations in groundwater levels. Nonetheless, its

secular rate tracks that of point 23 until 1997, at which point sample 75 begins to subside until by 2001 it is at a lower level than in 1992. This suggests at least some of sample 23's motion, particularly up to 1997, could also be groundwater related.
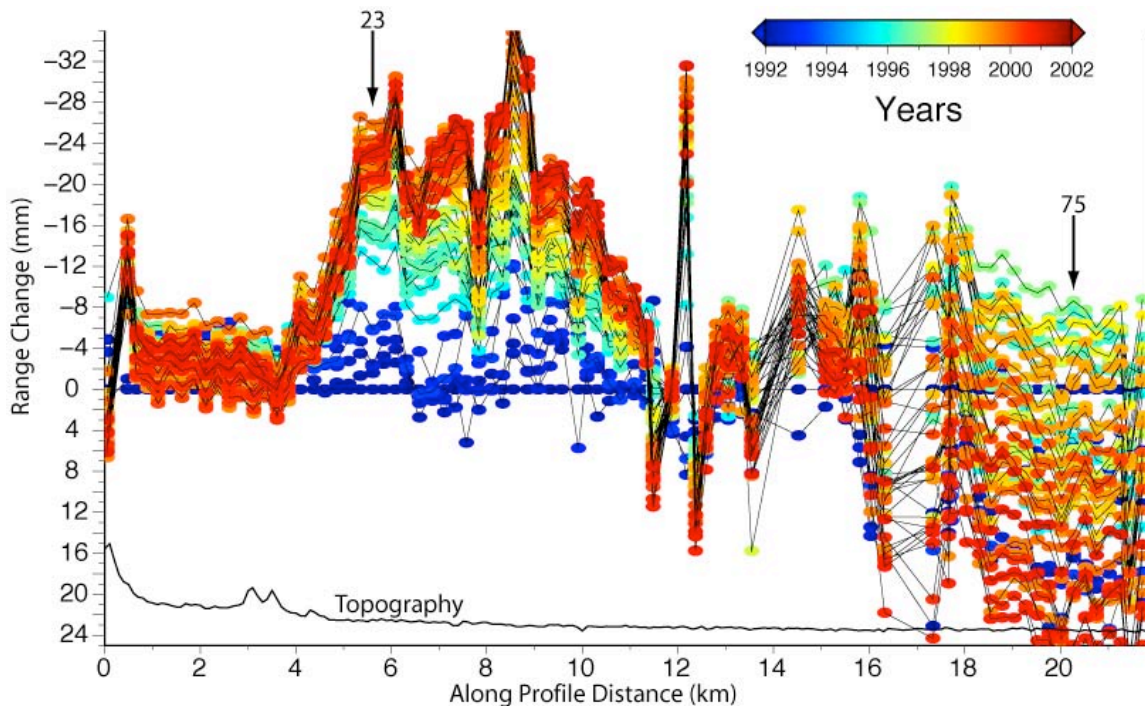

Figure 7 (above): Swath averages of PS-InSAR points within dashed box shown in Figure 6, and projected on to the centerline. Separate swath averages were calculated for each acquisition, which are colored by date. The locations of samples 23 and 75, discussed in the text, are marked by arrows. The black line at the bottom is normalized topography.
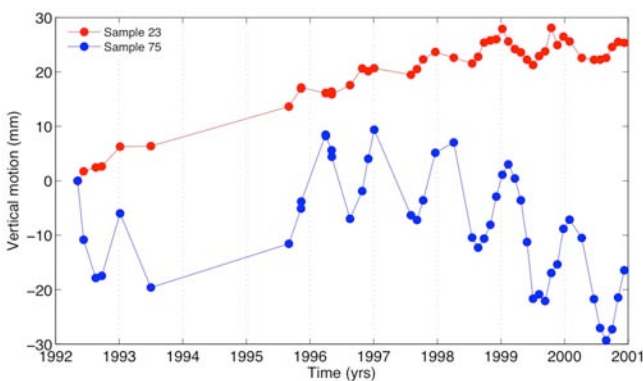
Figure 8 (left): Time series of motion for two points in the Vacaville profile. Sample 23 and 75 are swath average points marked in Figure 7.

Additionally, the shape of the Vacaville uplift feature does not match that expected from a buried dislocation. Figure 9 shows a profile from 1992-2001 with a forward model of a fault dipping 60° to the east, buried at a depth of 3 km and with a width of 7 km. The western limb of the anomaly is fit well by this model, but the eastern limb is not; the model rises less steeply than the data. It is worth also pointing out that the model requires a very shallow locking depth of 3 km, below which the fault would be creeping at a rate of 6.7 mm/yr (60 mm for the whole time span). A shallow locking depth is not consistent with large earthquake production, such as the 1892 M6.5 Vacaville-Winters earthquake, and would be unusual among Bay Area thrust faults.

Figure 9: Comparison of Vacaville profile from 1992-2001 to a forward model of a shallow east-dipping dislocation with a slip rate of 6.7 mm/yr. The western side of the profile is fit well, but the eastern side in not.
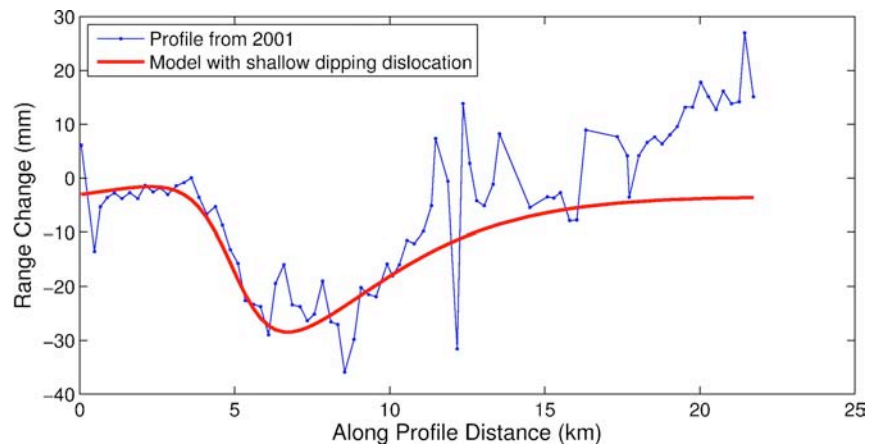
3.2 Mount Diablo Profile

The Mount Diablo (MD) thrust helps accommodate oblique convergence of the plate boundary and is inferred to connect the strike-slip Greenville and Concord faults where they form a restraining step-over. We investigate motions related to the MD thrust on a profile trending northeast-southwest, perpendicular to its strike (Figure 10).

Precisely measuring deformation, using PS-InSAR in the MD area, is difficult because of the scarcity of PS points on the mountain itself. This is a consequence of its steeper slopes and the lack of corner-reflecting buildings. The scarcity of the PSs is reflected in the increased scatter in the profiles (Figure 11) over MD and makes it difficult to determine if there is a consistent pattern of deformation in this area. Nonetheless, points northeast of MD show an increased range change rate consistent with uplift.

Apparent uplift northeast of MD can be seen in the motions of individual points (Figure 12). Points southwest of MD (samples 36 & 47) show little motion relative the reference location (small box in Figure 10). Sample 61, near the MD summit, shows motion consistent with subsidence. This would need to be investigated more closely, as the swath averages over Mount Diablo could be unduly influenced by a small number of anomalous points and/or points near the edge of the swath. Samples further north along the profile, consistently show an increase in apparent uplift rate.
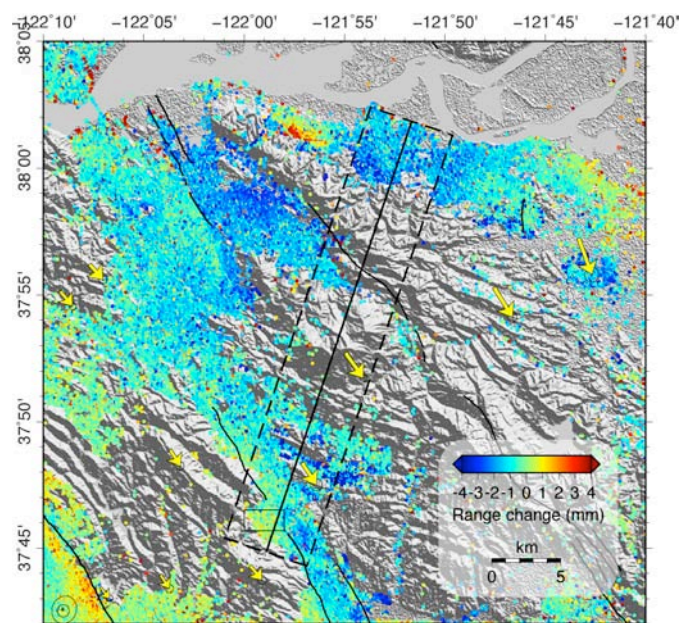

Figure 10: Map view with shaded topography, showing velocity of PS-InSAR points as colored circles. Yellow arrows are BAVU GPS velocities. Dashed box shows area used for swath averaging. Velocities are relative to the mean of points within the black box near the southwest end of the profile.

While the change in motion across MD is consistent with increased uplift rate, it could also be due to horizontal motions. In BAVU, GPS station DIAB, on MD's peak, has an average horizontal velocity of 5.7 ± 2.1 mm/yr (S28°E) relative to station WED2, just off the southwest edge of the MD swath in Figure 10. This translates into an apparent uplift rate of 1.6 ± 0.6 mm/yr; near the 1.2 ± 0.4 mm/yr range observed for Sample 92. Station JOBE has a horizontal velocity of 7.8 ± 2.4 mm/yr (S23°E) relative to WED2, which translates to 2.0 ± 0.6 mm/yr of apparent uplift. JOBE and Sample 111 are about equidistant to the Greenville fault trace, although they are significantly offset along strike. The complex deformation created by the restraining step-over from the Greenville to Concord faults may cause significant differences in the velocities at these two points and some uplift at Sample 111 cannot be ruled out. However the horizontal velocity of 5.7 ± 2.1 mm/yr observed constrains the maximum possible uplift observed using the PS-InSAR to no more than 0.6 ± 1.0 mm/yr.
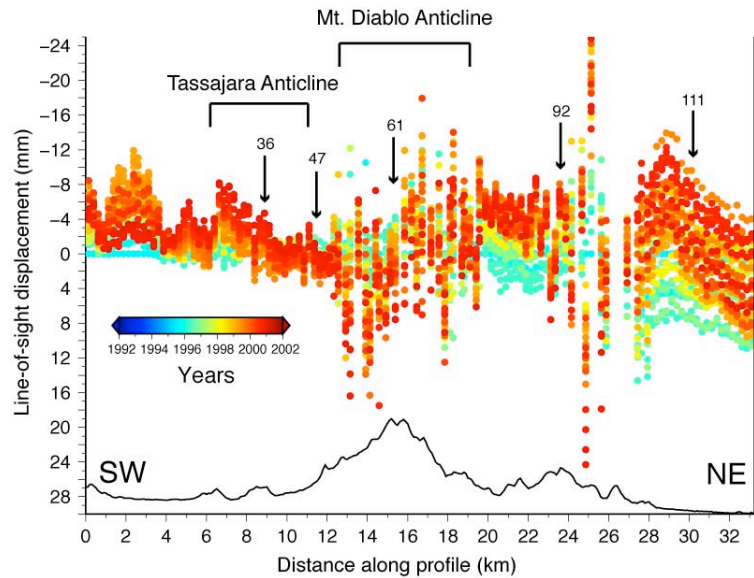

Figure 11: Swath averages of PS-InSAR points within dashed box shown in Figure 10. Separate swath averages were calculated for each acquisition, which are colored by date
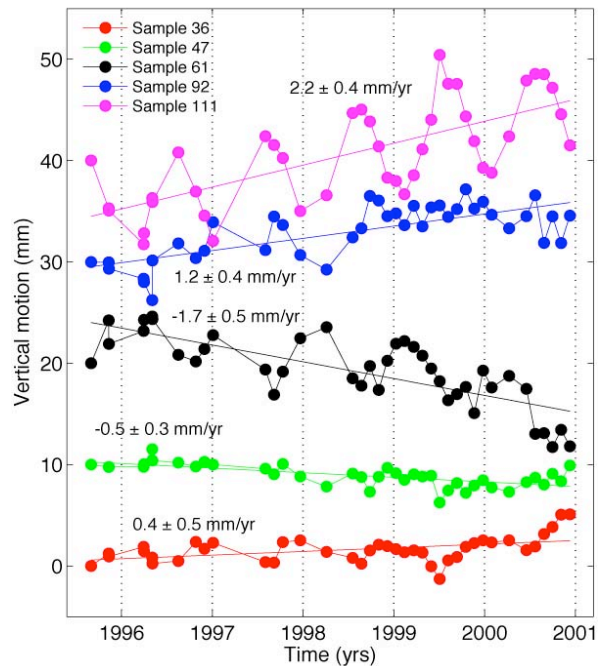

Figure 12: Time series of motion for five points in the Mount Diablo profile. The locations of the points along the swath average are marked in Figure 11. Solid lines are fit to the samples using a least-squares method; each line's slope is marked next to the time series.
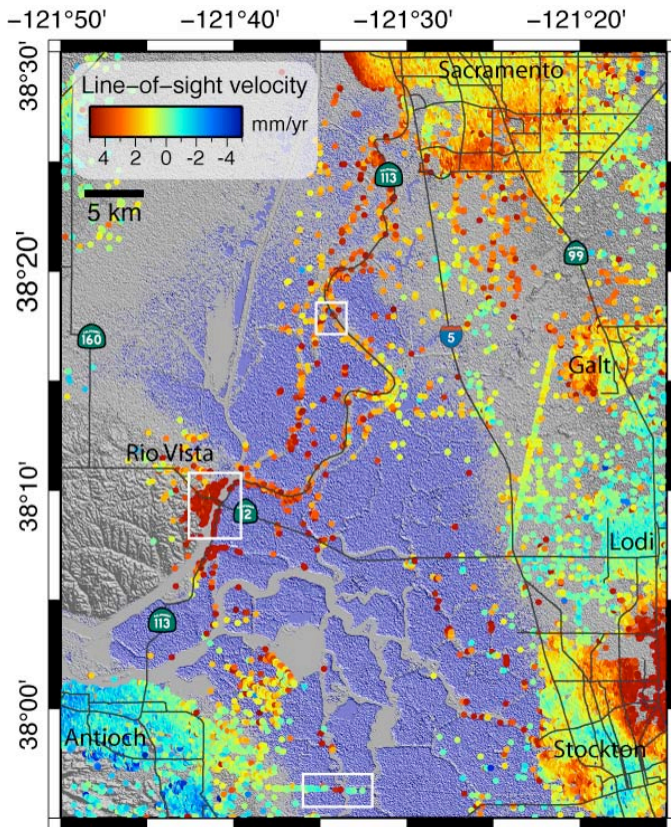
Figure 13: PS-InSAR over San Joaquin Delta. Blue areas lie below sea level, protected by levees along rivers and canals. Stable scatterers are sparse in agricultural areas.

3.3. San Joaquin Delta

The PS-InSAR data provide particularly valuable information on non-tectonic deformation and the integrity of the Delta levee system. We find rapid land subsidence of up to ~10 mm/yr in the Sacramento Delta region, including some of the levees that protect the low-lying area from flooding.

The ability of PSs to reveal precise locations where subsidence is occurring is demonstrated in the southern part of the Delta region. Here a series of PSs are located along a pipeline running East-West (lower white box in Figure 13). Most of these points are relatively stable as shown by their green color in Figure 13, however three points within this set show strong subsidence (red color). A close-up of this area in Google Earth reveals that although most of the points fall along the pipeline, one PS is located on the levee wall just to the north (Figure 14B). This is one of the subsiding points, with a range change rate of 3.2 mm/yr (subsidence of 3.5 mm/yr). The other two subsiding points are located where the pipeline approaches a waterway (Figure 14C). Here a small inlet containing boat docks forms a corner with water on two sides. Buildings near the boat docks provide two PS points that are clearly subsiding, one at a rate of 4.6 mm/yr (4.2 mm/yr range-change) and the point closer to the corner is subsiding at a rate of 7.7 mm/yr (7.1 mm/yr range-change).

The area of strongest subsidence is near the town of Rio Vista, which has a mean subsidence rate of 5.3 mm/yr, with some points up to 10 mm/yr. An abundance of PS points in the built areas show consistent subsidence of 4-6 mm/yr (Figure 14D). The surrounding area, including a bridge carrying Hwy 12 and the levees on the opposite shore show similar subsidence rates, though PSs on the levees towards the south show slightly higher rates of 7-8 mm/yr.

The levees around the Sacramento River also provide a high number of PS points and show high rates of subsidence in specific locations. Figure 14E shows that not only do PSs correspond to levees, but buildings within islands also provide PS points and show that these inland areas are also subsiding.
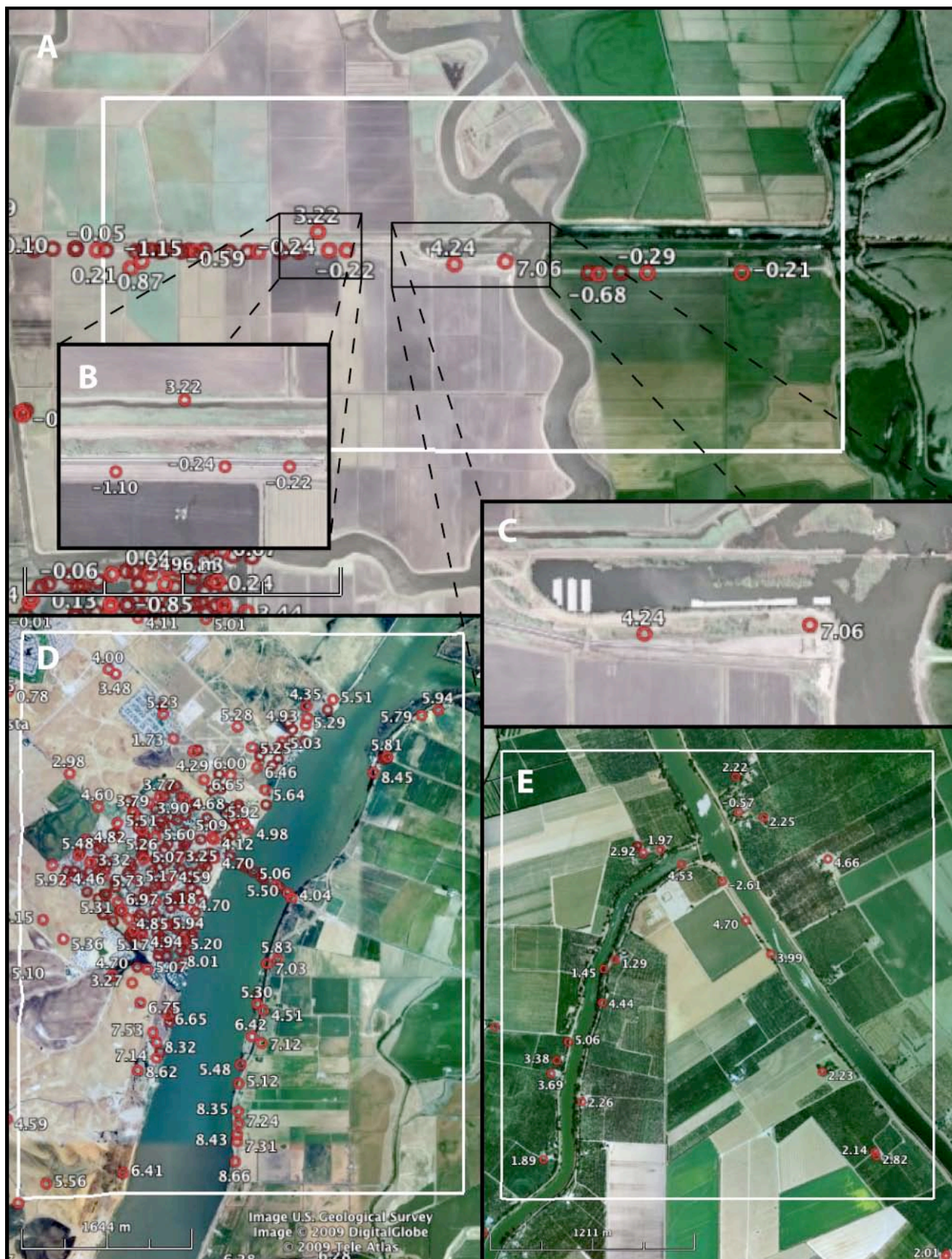
Figure 14 (previous page): Close-ups of PS point locations using Google Earth with label indicating range-change rate. Multiply these rates by -1.086 for equivalent vertical rates. White boxes correspond to boxes in Figure 13. A) An aqueduct provides a linear series of PS points. B) There is a difference in motion between the relative stable pipeline PS points and the subsiding levee. C) Here, rate of subsidence is related to distance from to the main waterway. The point on the corner, with water on two sides has a higher subsidence rate than the inland point. D) PS points surrounding the town of Rio Vista E) PS point locations along the Sacramento River.

3.4. Concord Fault

To measure creep on the Concord fault, we look at motion along several profiles through the PSs crossing the Concord fault. We use swath averaging to construct each profile. Within each swath, shown as dashed lines in Figure 15, points within 0.25 km bins perpendicular to the fault are averaged together and projected onto the centerline. For example, all points between 0.5 and 0.75 km west of the fault are averaged together to provide one point on the profile and their standard deviation provides an estimate of the profile point's uncertainty.

Figure 15: Overview map showing mean velocity of each PS-InSAR points from 46 InSAR scenes spanning 1992-2001. Dashed boxes are the areas included in the swath averages, which are then projected onto the solid black centerlines. The two alinement arrays, CSAL and CASH, are shown as white triangles and fall mostly within Profile 3 (P3).

A swath average profile is constructed for all 46 acquisition dates for Track 70, Frame 2853 on each of the five profiles, for a total of 230 profiles. We model the fault creep as simple block motion, which should produce an offset at the fault trace and little off-fault deformation.

A linear inversion is performed to fit each profile with a model that includes an offset at the fault and straight line segments on either side (an example is shown in Figure 16). The modeled offsets represent the cumulative amount of creep on the Concord fault since the beginning of the time series in 1992.

The modeled profile offsets give us time series of fault creep at the five locations (Figure 17). The offsets are in turn be fit by a line to obtain an estimate of the long-term creep rate at
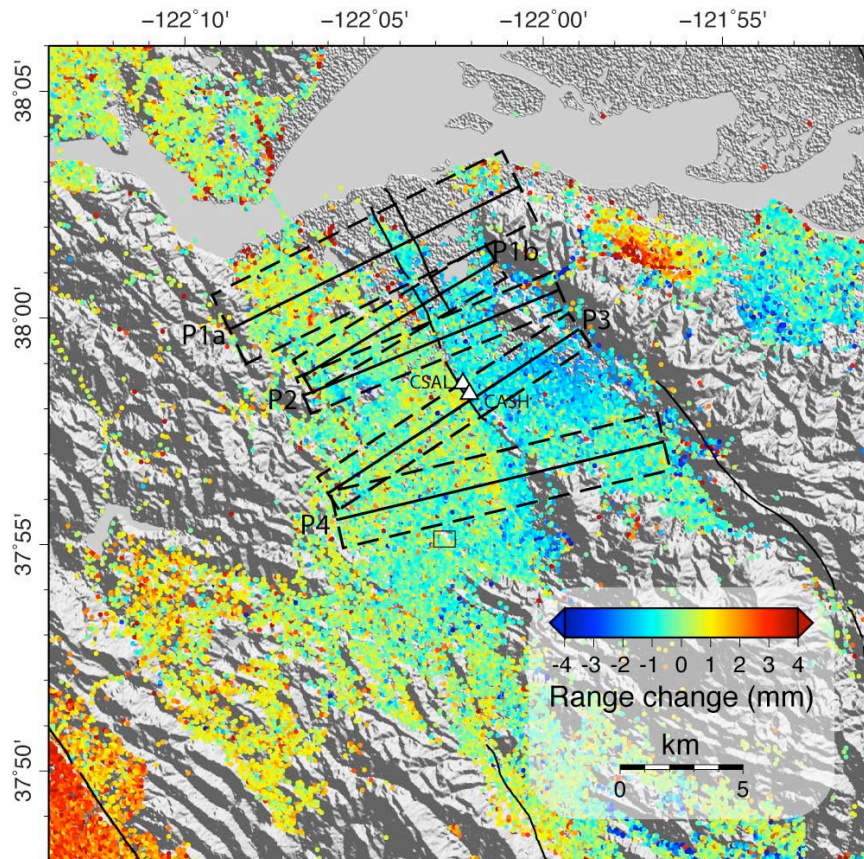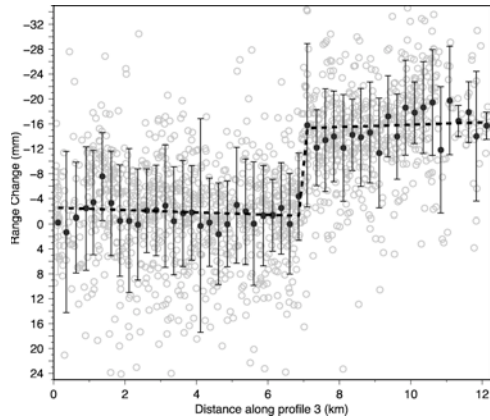
Figure 16 (above): An example of a swath average profile; this is for profile 3 on 12/9/2001, referenced to 5/6/1992. Grey circles are the actual PS-InSAR points within the dashed box in Figure 15 and projected onto the centerline. Black circles are the derived swath averages; averages of all points inside a 0.25 km bin. Error bars are one standard deviation of the PS-InSAR points comprising each swath average. The dashed black line is fit to the data using a linear inversion and the fault creep is measured from the offset of the profile at the fault trace.
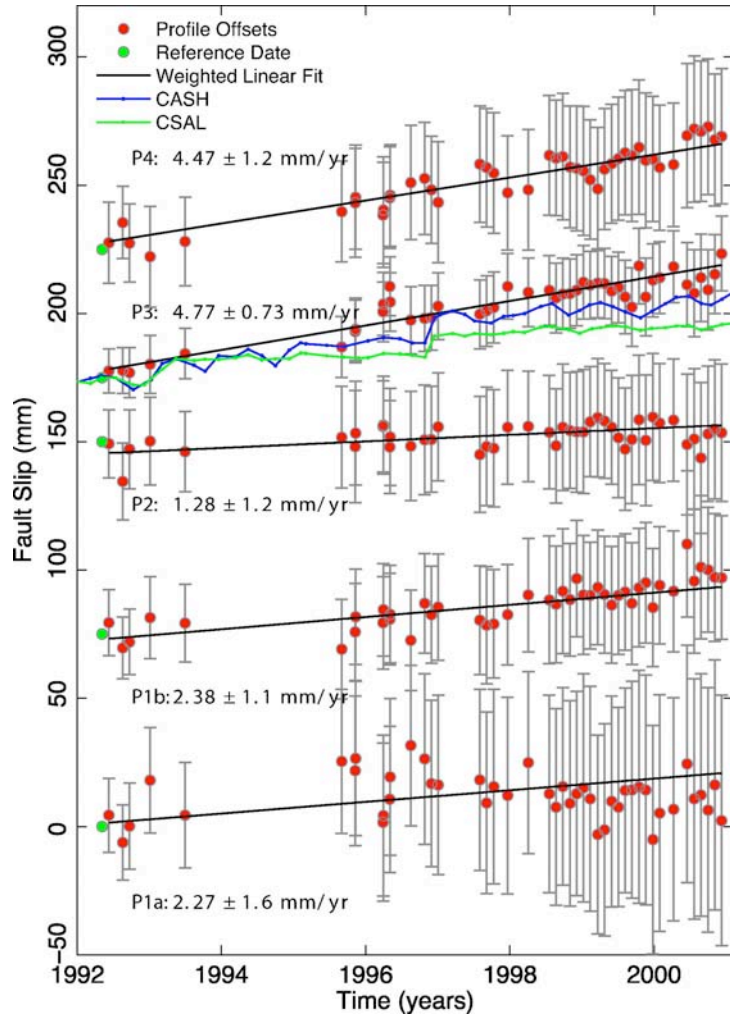

Figure 17 (right): Surface creep through time for the five profiles shown in Figure 15. Individual time series are offset from each other for clarity. The creep rate as determined from a weighted linear inversion is printed next to each series. Alinement array measurements from sites CSAL and CASH are plotted with Profile 3 (P3) for comparison

each profile. The two northern-most profiles (P1a & P1b) have creep rates of 2.3-2.4 mm/yr; this is very low, but measurable within the calculated uncertainty of 1.1-1.6 mm/yr. The creep rate continues to be low southward through profile 2 (P2), where the measured rate could be zero within uncertainty. Creep picks up fairly suddenly at profile 3 (P3), which is near the portion of the fault known to creep from alinement arrays. Time series of creep measurements from the alinement arrays are plotted with the time series from P3 in Figure 17. Both arrays measure slightly lower creep rates than is indicated by P3, but support the idea that the creep rate is increasing toward the south. CSAL is the more northern alinement array and is on the north edge of P3 (see Figure 15); it has a lower creep rate (2.8 mm/yr) than CASH (3.7 mm/yr), which is located toward the center of P3. P3 incorporates more data to the south of CASH, which may explain its higher creep rate. Higher rates of creep continue in profile 4 (P4), our southern-most profile.

Creep on the Concord fault has also been shown by alinement array measurements to be episodic, with a 3-5 year period. This variability is within the uncertainty in the profile offsets and could not be independently detected using the PS-InSAR data. However, offsets for P3 match some of the variability in alinement array CASH, particularly post-1998, suggesting that there is information available in the PS-InSAR data on the time variability of Concord fault creep.

References

Argus, D. F., and R. G. Gordon (2001), Present tectonic motion across the Coast Ranges and San Andreas fault system in Central California, Geological Society of America Bulletin, 113, 12, 1580-1592.

Aydin, A., and B. M. Page (1984), Diverse Pliocene-Quaternary tectonics in a transform environment, San Francisco Bay region, California, Geological Society of America Bulletin, 95, 11, 1303-1317.

Bennett, J. H. (1987), Vacaville-Winters earthquakes, 1892; Solano and Yolo counties, California Geology, 40, 4, 75-83.

Bürgmann, R., G. Hilley, A. Ferretti, and F. Novali (2006), Resolving vertical tectonics in the San Francisco Bay area from permanent scatterer InSAR and GPS analysis, Geology (Boulder), 34, 3, 221-224.

Colesanti, C., A. Ferretti, F. Novali, C. Prati, F. Rocca, and Anonymous (2003), SAR monitoring of progressive and seasonal ground deformation using the permanent scatterers technique, IEEE Trans Geosci Remot Sen, 41, 7, Part 1, 1685-1701.

d'Alessio, M. A., I. A. Johanson, R. Bürgmann, D. A. Schmidt, and M. H. Murray (2005), Slicing up the San Francisco Bay Area: Block kinematics and fault slip rates from GPS-derived surface velocities, Journal of Geophysical Research, 110, B06403.

Ferretti, A., F. Novali, R. Bürgmann, G. Hilley, and C. Prati (2004), InSAR permanent scatterer analysis reveals ups and downs in San Francisco Bay area, Eos, Transactions, American Geophysical Union, 85, 34, 317.

Ferretti, A., C. Prati, and F. Rocca (2000), Nonlinear subsidence rate estimation using permanent scatterers in differential SAR interferometry, IEEE Trans Geosci Remot Sen, 38, 5 PT1, 2202-2212.

Ferretti, A., C. Prati, and F. Rocca (2001), Permanent scatterers in SAR interferometry, IEEE Trans. Geosci. Remote Sens. (USA), 39, 1, 8-20.

Freymueller, J. T., M. H. Murray, P. Segall, and D. Castillo (1999), Kinematics of the Pacific-North America plate boundary zone, Northern California, Journal of Geophysical Research, 104, B4, 7419-7441.

Hilley, G. E., R. Burgmann, A. Ferretti, F. Novali, and F. Rocca (2004), Dynamic of slow-moving landslides from Permanent Scatterer analysis, Science, 304, 5679, 1952-1955.

Murray, J., and P. Segall (2002), Testing time-predictable earthquake recurrence by direct measurement of strain accumulation and release, Nature, 419, 6904, 287-291.

Murray, M. H., and P. Segall (2001), Modeling broadscale deformation in Northern California and Nevada from plate motions and elastic strain accumulation, Geophysical Research Letters, 28, 22, 4315-4318.

O'Connell, D. R. H., J. R. Unruh, and L. V. Block (2001), Source characterization and ground-motion modeling of the 1892 Vacaville-Winters earthquake sequence, California, Bulletin of the Seismological Society of America, 91, 6, 1471-1497.

Page, B. M., D. C. Engebretson, and Anonymous (1984), Correlation between the geologic record and computed plate motions for Central California, Tectonics, 3, 2, 133-155.

Pollitz, F. F., and M. Nyst (2005), A physical model for strain accumulation in the San Francisco Bay region, Geophysical Journal International, 160, 1, 302-317.

Prescott, W. H., J. C. Savage, J. L. Svarc, and D. Manaker (2001), Deformation across the Pacific-North America plate boundary near San Francisco, California, Journal of Geophysical Research, 106, B4, 6673-6682.

Savage, J. C., W. Gan, W. H. Prescott, and J. L. Svarc (2004), Strain accumulation across the Coast Ranges at the latitude of San Francisco, 1994-2000, Journal of Geophysical Research, B, Solid Earth and Planets, 109, 3, 11.

Savage, J. C., R. W. Simpson, and M. H. Murray (1998), Strain accumulation rates in the San Francisco Bay area, 1972-1989, Journal of Geophysical Research, 103, B8, 18,039-018,051.

Unruh, J. R., T. A. Dumitru, and T. L. Sawyer (2007), Coupling of early Tertiary extension in the Great Valley forearc basin with blueschist exhumation in the underlying Franciscan accretionary wedge at Mount Diablo, California, Geological Society of America Bulletin, 119, 11-12, 1347-1367.